Asian Journal of Chemistry; Vol. 27, No. 3 (2015), 1102-1106

ASIAN JOURNAL OF CHEMISTRY

http://dx.doi.org/10.14233/ajchem.2015.18349

Silicon Nanowires/Pt for Enhanced Photo-Electrochemical Water Splitting Properties

TIANHAO XU, ZHIYI LU*, YINGJIE LI, HAIJUN XU, LIREN WANG* and XIAOMING SUN

State Key Laboratory of Chemical Resource Engineering, Beijing University of Chemical Technology, Beijing, P.R. China

*Corresponding authors: Tel: +86 010 6443899; E-mail: zhiyilu1124@gmail.com; wanglr@mail.buct.edu.cn

Received: 19 June 2014; *Accepted*: 19 September 2014; *Published online*: 19 January 2015; AJC-16734

Incorporation of co-catalysts onto silicon-based nanomaterials has been diligently pursued as photocatalysts for water splitting. Here we employ a metal-assisted chemical etching method to fabricate different types (p type and n type) of silicon nanowire arrays (Si NWs), followed by the Pt deposition outside. The resulting Si NWs/Pt exhibits much enhanced photo-electrochemical properties, with higher photocurrent density and lower onset potential relative to the pristine silicon nanowire arrays and planar silicon due to the high surface roughness of silicon nanowire arrays and the addition of Pt catalyst. We have also demonstrated that different types of Si NWs/Pt show different enhancement effects for oxygen evolution reaction and hydrogen evolution reaction under illumination. This study demonstrates an excellent photo-electrochemical catalyst for water splitting and provides a valuable guidance for choosing the right type of silicon in terms of the target chemical reaction.

Keywords: Silicon nanowires, Silicon type, Photo-electrocatalysis.

INTRODUCTION

The majority of energy (electricity, hydrogen *etc*.) are produced from fossil fuels, which are believed to be the major cause of negative and irreversible environmental consequences, such as greenhouse gas emission and air pollution. Direct splitting of water using semiconductor materials under solar irradiation to produce clean and recyclable energy carrier on a large scale would be one of the best ways to solve the problems of energy shortages and environmental pollution[1-5]. Many kinds of materials have been studied for photo-electrochemical reactions[6], such as ZnO[7], Fe_2O_3[8], Ta_3N_5[9]. Of all the semiconductor photo-electrochemical materials, silicon as a kind of earth abundant semiconductor gains extensive attention in the field of light harvesting because silicon possesses a narrow band gap (Eg = 1.12 eV), which enables the absorption of the solar radiation energy ranging from ultraviolet to visible light[10]. Meanwhile silicon nanowire arrays (Si NWs) as a kind of one-dimensional semiconductor nanostructures exhibits promising application potential in the field of photo-electrochemistry because of their remarkably improved optical absorption or/and charge collection ability in comparison with the bulk materials and zero-dimensional nanostructures[11-16]. In addition, nanostructure can introduce changes in the semiconductor energetics that can enhance the semiconductor/electrolyte characteristics. However, the performances of silicon-based devices are usually limited by slow kinetics at the silicon-electrolyte interface. The introduction of noble metal particles (*e.g*., Pt) to the surface of planar silicon or silicon nanowire has been proved to be an efficient approach for the improvement of their photo-electrochemical performance[17-19]. At the same time the surface modification with other electrocatalysts (*e.g*., Ni-Mo[20], Mo_3S_4 clusters[21] and reduced graphene oxide[22]) or surface energy band engineering (*e.g*., /Fe_2O_3[23,24], Si NWs/TiO_2[25], Si NWs/Cu_2O[26] and Si NWs/ZnO[27] nanowire heterostructures) can also improve the photo-electrochemical performance of the silicon-based devices.

Herein, silicon nanowire arrays incorporated with Pt nanoparticles were fabricated by metal-assisted chemical etching (MACE)[28] and subsequent Pt deposition for both p- and n-type substrates (The substrates were both <100> oriented). As the integrated electrodes for water splitting, the resulting Si NWs/Pt exhibited much enhanced photo-electrochemical properties, including higher photocurrent density and lower onset potential than that of pure silicon nanowire arrays and the planar silicon for both oxygen evolution reaction (OER) and hydrogen evolution reaction (HER). Moreover, we have demonstrated that the Si NWs/Pt fabricated by different types silicon substrate showed completely different consequences under illumination for diverse reactions. The Si NWs/Pt prepared by p-type silicon substrate (p-Si NWs/Pt) was found to be more active for hydrogen evolution reaction, whereas the Si NWs/Pt prepared by n-type silicon substrate (n-Si NWs/Pt) was more suitable for oxygen evolution reaction. The

relationship between the type of the silicon and type of electrochemical reaction (oxygen evolution reaction and hydrogen evolution reaction) was also revealed. Combination of the good photo-electrochemical performance of Si NWs/Pt and the completely different performance caused by the type of the substrate for oxygen evolution reaction and hydrogen evolution reaction endow this work as a valuable study for further exploration of high active materials and screening the silicon substrate type for different reaction.

EXPERIMENTAL

All the reagents used in the experiment were analytically pure and used without further purification.

The silicon nanowire arrays were fabricated *via* metal-assisted chemical etching (MACE) method. Two kinds of silicon wafer were used in this article, p-type (<100> oriented, 10^{-2}-10^{-3} Ω cm) and n-type (<100> oriented, 10^{-2}-10^{-3} Ω cm). The wafer (1 × 4 cm^2) was degreased by ultrasonication in sequence in water, ethanol and acetone each for 5 min and then rinsed with copious amount of deionized water. Afterward, the degreased silicon wafers were used in a typical metal-assisted chemical etching process, the cleaned silicon substrates were immersed in an $AgNO_3$/HF solution ($AgNO_3$, 40 mg; HF, 15 mL; H_2O, 25 mL) for electroless deposition of Ag nanoparticles (Ag NPs) at room temperature about 2 min. Subsequently the Ag NPs-coated silicon chips were immersed into the H_2O_2/HF (HF, 15 mL; H_2O_2, 2 mL; H_2O, 25 mL) solution for chemical etching about 0.5 h. Finally, the as-etched silicon nanowire arrays were cleaned with de-ionized water and dried naturally in air. Surface becomes darkened due to silicon nanowire formation. In order to impregnate the silicon nanowire with Pt catalyst, the silicon nanowire sample was immersed into a HF/H_2PtCl_6 (H_2PtCl_6, 0.04 mmol; HF, 10 mL; H_2O, 20 mL) solution for 3 min, then rinsing with de-ionized water and drying naturally in air.

SEM images were taken on a Zeiss SUPRA55 scanning electron microscope (SEM) with an accelerating voltage of 20 kV. X-ray diffraction (XRD) datas were collected with a Rigaku UItima III diffractometer using monochromatic CuK_α radiation (λ = 0.15418 nm). The reflectance spectra of planar silicon and Si NWs/Pt samples were measured on a SHIMADZU UV-3600 UV-visible-near IR spectrophotometer.

Photo-electrochemical measurement: The photo-electrochemical measurements of different types planar Si, silicon nanowire arrays and Si NWs/Pt were carried out in 0.5 M H_2SO_4 solution with an electrochemical workstation (CHI 660D, CH Instrument) at a scan rate of 20 mV/s. A three-electrode configuration was adopted in the measurements, with different type Planar Si, silicon nanowire arrays or Si NWs/Pt as the working electrode, a Pt foil (1 × 1 cm^2) as the counter electrode and a Ag/AgCl reference electrode as the reference electrode. The reversible hydrogen evolution potential (RHE) was measured in the same solution using a clean Pt electrode as the working electrode and Ag/AgCl as the reference electrode, being -0.202 V *vs*. Ag/AgCl. Therefore, a potential measured with respect to the Ag/AgCl electrode was referenced to RHE by adding a value of 0.202 V. The samples were assembled into a homemade electrochemical cell, with only a defined area (1 cm^2) of the sample exposed to the solution during measurements. For photo-electrochemical measurement, a xenon lamp was used as the light source. The power of the light can be controlled and was determined by a thermopile detector.

RESULTS AND DISCUSSION

The silicon nanowire arrays were fabricated by the HF corrosion and Si NWs/Pt composites were obtained using HF to reduce H_2PtCl_6 on the silicon nanowire arrays. The morphologies of the silicon nanowire arrays prepared by different types of substrates were almost the same and the average length and width were around 3 μm and 50 nm after 0.5 h of etching, respectively. After deposition of Pt nanoparticles, the surface morphologies preserved well for both n-Si NWs/Pt and p-Si NWs/Pt, as shown in Fig. 1A and B. The as-deposited Pt nanoparticles tended to aggregate on the tips of the silicon nanowire arrays which can be seen in Fig. 1C and D, indicating these areas were mostly accessible for catalyst deposition. The average diameter of the Pt nanoparticles was 20 nm. The above results indicated that the surface roughness of the silicon nanowire dramatically increased in compared with planar silicon and the deposited Pt should also make the surface rougher. The high roughness surface brought a large specific area and excellent light absorption performance, which would be the crucial factors to enhance the photo-electrochemical performance.

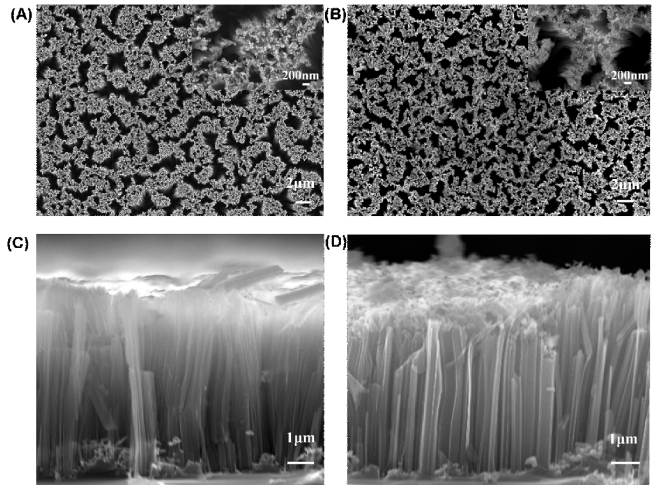

Fig. 1. Typical plane view (top row) and cross-sectional view (bottom row) SEM images of different types Si NWs/Pt. (A) top view of p-Si NWs/Pt, together with the corresponding high magnification, shown in the inset; (B) top view of n-Si NWs/Pt, inset is the high magnification SEM image; (C) cross-sectional view of p-Si NWs/Pt; (D) cross-sectional view of n-Si NWs/Pt

The XRD pattern of the as-prepared Si NWs/Pt showed the unusual strong peak located at about 68° corresponded to the Si (400) plane of the silicon nanowire arrays, which indicated a strong orientation along the c-axis of the silicon nanowire arrays (Fig. 2). Besides the silicon peak, we can also observe 2 minor peaks at about 40° and 46°, whose positions and relative intensities were found to identify the Pt (111) and (200) planes, respectively. The EDS spectrum of the Si NWs/Pt revealed a relative content of 40:1 for Si and Pt, thus

indicating a low mass-loading of precious Pt which was well agreed with the XRD result.

The photo-electrochemical property of the as-prepared Si NWs/Pt was carried out using a typical three-electrode setup in aqueous 0.5 M H_2SO_4 solution. For comparison purposes, the catalytic activities of different types of pure silicon nanowire arrays and planar silicon were also investigated. It was found that under illumination, both n-type and p-type Si NWs/Pt exhibited the largest current density comparing with the silicon nanowire arrays and planar Si. The silicon nanowire arrays also showed a better performance than that of the planar Si. This sequence was suitable for both the hydrogen evolution reaction and oxygen evolution reaction. The highest photo-electrocatalytic performance of Si NWs/Pt was attributed to the unique architecture of silicon nanowire arrays which provided the largest surface area and highest light absorption behaviour and the deposition of Pt nanoparticles which acted as an active component of the photo-electrocatalysts. The light enhanced performance of n-Si NWs/Pt and p-Si NWs/Pt for hydrogen evolution reaction and oxygen evolution reaction when exposed to the illumination with an intensity of 100 mW cm^{-2} were investigated and shown in Fig. 3. It should be noted that n-Si NWs/Pt and p-Si NWs/Pt showed totally different enhancements for hydrogen evolution reaction and oxygen evolution reaction, respectively. For hydrogen evolution reaction (Fig. 3A), the n-Si NWs/Pt showed a better performance than the p-Si NWs/Pt in terms of the onset potential and the photo current density in the dark. However, the p-Si NWs/Pt exited obviously enhanced performance under the conditions of the light with a positive shift about 250 mV of the onset potential, whereas the n-Si NWs/Pt exhibited almost the same before and after the light illumination with a slight change of 10 mV. The photo current density of the p-Si NWs/Pt reached to about 1.68 mA cm^{-2} at 0 V *vs*. reversible hydrogen electrode (RHE). As for the oxygen evolution reaction (Fig. 3B), completely reverse phenomena were observed. The p-Si NWs/Pt showed a better performance than the n-Si NWs/Pt in the dark, while the performance of n-Si NWs/Pt was significantly improved and exceeded that of p-Si NWs/Pt under illumination.

The above results demonstrated that the Si NWs/Pt showed a better performance than the silicon nanowire arrays and the planar silicon for both hydrogen evolution reaction and oxygen evolution reaction under illumination. The observation is caused by the large specific area and the unique structure of the silicon nanowire arrays which can enhance the light adsorption and the introduction of Pt co-catalyst which benefits

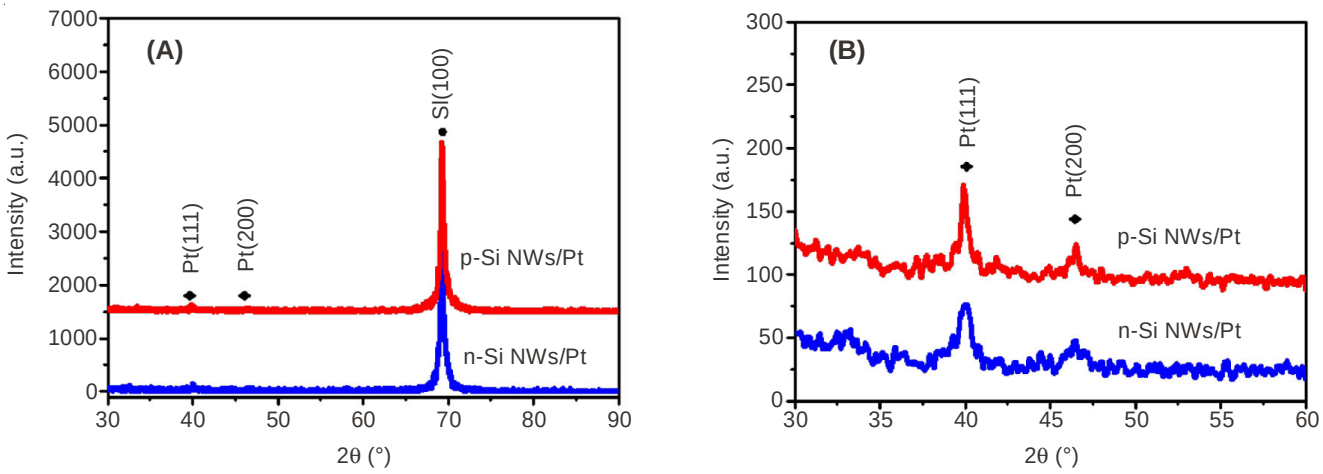

Fig. 2

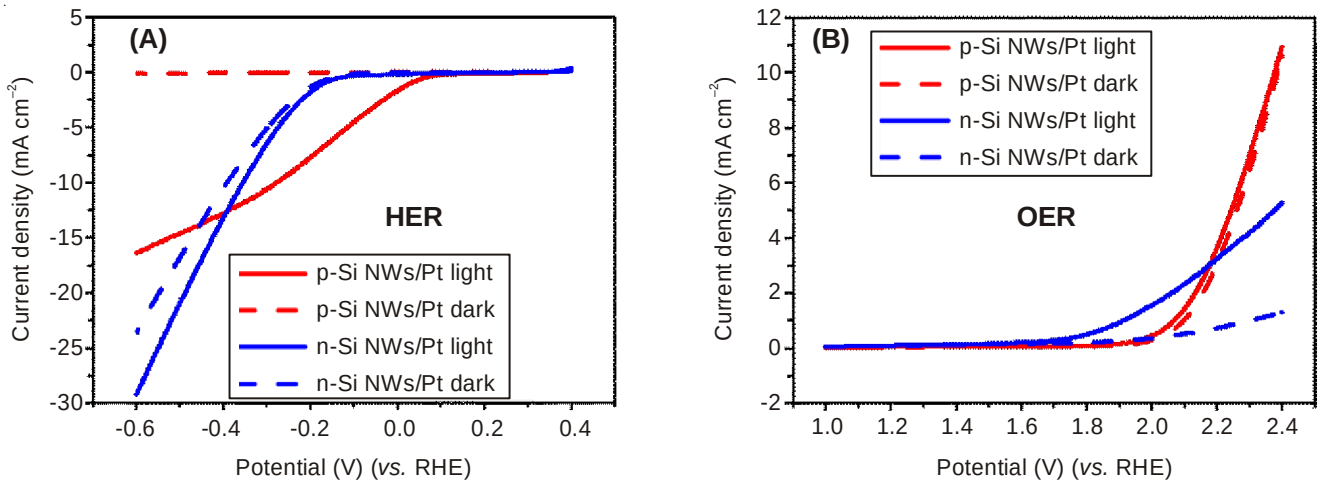

Fig. 3. Photo-electrochemical performance of n-Si NWs/Pt and p-Si NWs/Pt with and without light, the solid lines are the LSV curves under lighting conditions and the dotted lines are the LSV curves in the dark. (A) The HER performance of the Si NWs/Pt; (B) The OER performance of the Si NWs/Pt

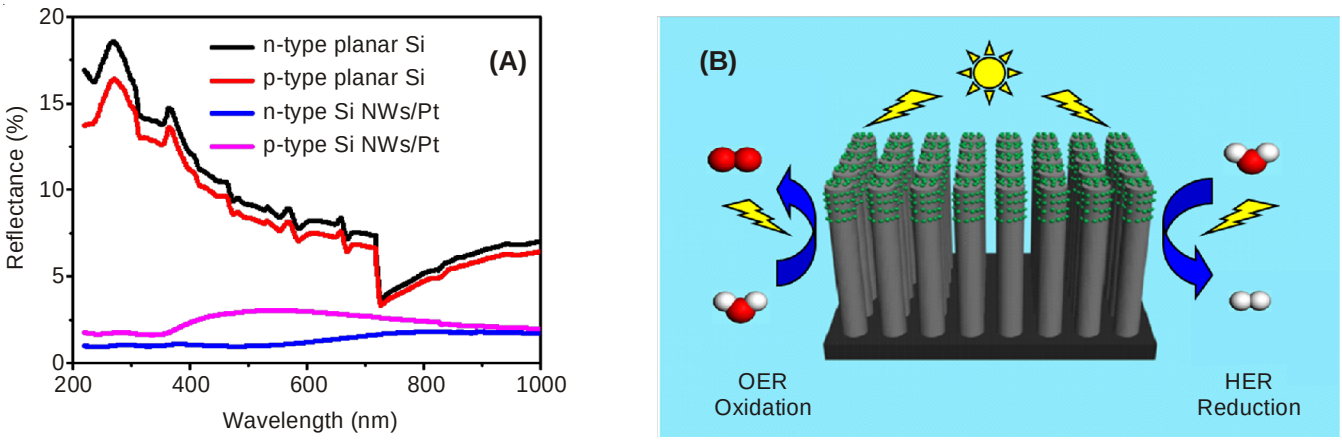

Fig. 4. (A) Reflectance spectra of different types planar Si and Si NWs/Pt samples. (B) Schematic picture of Si nanowire array photoelectrode. Photon absorbed by Si nanowire generates minority carrier (electron or hole), which drifts to semiconductor/electrolyte interface where H_3O^+ is reduced to H_2 (electron) and OH^- is oxided to O_2 (hole). Si nanowire is impregnated with Pt nanoparticles that serves as electrocatalysts for the electrode reaction. (The red atom is O, the white atom is H, the green is Pt and the gray is the Si)

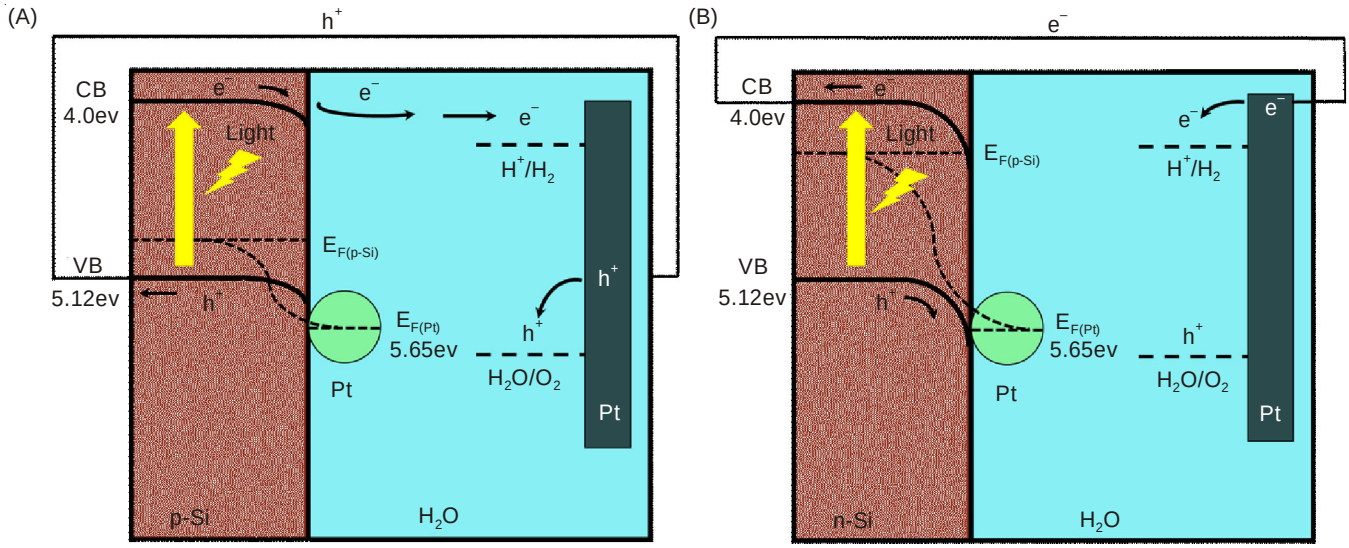

Fig. 5. Schematic drawing of the band gap structure of the p type Si NWs/Pt (A) and n type Si NWs/Pt (B), and a tentative flow of the carriers under the conditions of the light for water splitting. CB = conduction band, VB = valence band, EF = Fermi level, EF(Pt) = Fermi level of Pt, EF(p-Si) = Fermi level of p-Si, EF(n-Si) = Fermi level of n-Si. All the values are *vs*. vacuum level

the separation of the charge/hole pair and thus increases the efficiency. The excellent light adsorption property can be explained by the optical performance of the Si NWs/Pt. Fig. 4A showed the reflectance spectra of the as-prepared n-Si NWs/Pt, p-Si NWs/Pt, planar n-Si and p-Si. The reflectance of n-Si NWs/Pt and p-Si NWs/Pt were less than 3% within a wavelength interval of 220-1000 nm, while reflectance of the planar silicon was in a range of 10 to 20 % with the same wavelength. These results indicated that the as-prepared Si NWs/Pt exhibited an excellent light absorption performance due to the light trapping effects of the highly-porous nanowire array structure which was consistent with the SEM results. Therefore, we hypothesize that this Si NWs/Pt structure is more desirable for photo-electrochemical catalysis (Fig. 4B).

The introduction of Pt could also greatly improve the photo-electrochemical performance, which was attributed to the band engineering of the silicon nanowire arrays. The possible mechanisms were schemed in Fig. 5. Under illumination, the conductive band (CB) and valence band (VB) of different type silicon were downshifted at the surface with different band bending due to the existence of Pt outside. For the hydrogen evolution reaction reaction (Fig. 5A), a small band bending happened for the p-Si, thus the photo-generated electron in the conductive band of silicon nanowire arrays could be transferred from the surface to the electrolyte to reduce protons through Pt. The Pt can facilitate the electron transportation and thus effectively restrain the recombination of electron/hole pair. As a result, a relatively large number of electrons were involved in the catalysis reaction, indicating a fast kinetic for hydrogen evolution reaction. The residual holes would be transferred to the counter electrode for generating O_2. Accordingly, the p-Si NWs/Pt showed a more positive onset potential in hydrogen evolution reaction under illumination. As for the n-type silicon, the band structure bending was much larger than the p-Si (Fig. 5B), which made the n-typed Si NWs/Pt more desirable for oxygen evolution reaction. The holes in the VB were easier to transfer from the surface to electrolyte to convert the OH- to O_2. Note that the n-Si NWs/Pt was not

as active as other active components decorated on silicon nanowire arrays photo-electrocatalysts (*e.g*. Si NWs/Fe_2O_3[24]), which was due to the sluggish oxygen evolution reaction kinetic of Pt. However, in this study we have clearly demonstrated the suitable choice of silicon for specific catalysis reactions, which would give some advices for further optimizing the performance.

The relationship between the light intensity and the photo-electrocatalytical activity was further studied. The results indicated that enhancing the light intensity to the p-Si NWs/Pt could improve the hydrogen evolution reaction performance while the n-Si NWs/Pt the hydrogen evolution reaction performance changed little when the light intensity changed. As for the oxygen evolution reaction, the opposite result was observed. The n-Si NWs/Pt exhibited a significantly improved performance when the light intensity was increased and the p-Si NWs/Pt almost kept the same. The above results further confirmed that the p-type silicon was suitable for hydrogen evolution reaction while n-type silicon was desirable for oxygen evolution reaction.

Conclusion

In summary, different types Si NWs/Pt were fabricated *via* a convenient metal-assisted chemical etching method, followed by Pt deposition at the outside of silicon nanowire arrays. The Si NWs/Pt exhibited significantly improved photo-electrochemical water splitting properties, in comparison with the pristine silicon nanowire arrays and planar silicon samples. The enhancement of photo-electrochemical performance can be attributed to the large specific surface area of silicon nanowire arrays and the addition of the Pt co-catalyst. We have also studied that the relationship between the type of silicon substrates and the type of the photo-electrocatalytic reaction and found that different types of Si NWs/Pt showed different enhancement for oxygen evolution reaction and hydrogen evolution reaction under illumination. This study not only offers a practical route for synthesizing Si NWs/Pt nanocomposites with high photo-electrochemical performance, but also provides a new guidance in screening the right type of silicon substrate in terms of the type of the target chemical reactions.

REFERENCES

1. S.Y. Reece, J.A. Hamel, K. Sung, T.D. Jarvi, A.J. Esswein, J.J.H. Pijpers and D.G. Nocera, *Science*, **334**, 645 (2011).
2. A. Kudo and Y. Miseki, *Chem. Soc. Rev*., **38**, 253 (2008).
3. M. Gratzel, *Nature*, **414**, 338 (2001).
4. M.J. Kenney, M. Gong, Y.G. Li, J.Z. Wu, J. Feng, M. Lanza and H. Dai, *Science*, **342**, 836 (2013).
5. Y.W. Chen, J.D. Prange, S. Duhnen, Y. Park, M. Gunji, C.E.D. Chidsey and P.C. McIntyre, *Nat. Mater*., **10**, 539 (2011).
6. M.G. Walter, E.L. Warren, J.R. McKone, S.W. Boettcher, Q. Mi, E.A. Santori and N.S. Lewis, *Chem. Rev*., **110**, 6446 (2010).
7. Y.K. Hsu, S.Y. Fu, M.H. Chen, Y.-C. Chen and Y.-G. Lin, *Electrochim. Acta*, **120**, 1 (2014).
8. G. Rahman and O.S. Joo, *Int. J. Hydrogen Energy*, **37**, 13989 (2012).
9. X.J. Feng, T.J. LaTempa, J.I. Basham, G.K. Mor, O.K. Varghese and C.A. Grimes, *Nano Lett*., **10**, 948 (2010).
10. K.Q. Peng, Y. Xu, Y. Wu, Y. Yan, S.-T. Lee and J. Zhu, *Small*, **1**, 1062 (2005).
11. B.M. Kayes, H.A. Atwater and N.S. Lewis, *J. Appl. Phys*., **97**, 114302 (2005).
12. K.Q. Peng, X. Wang, X.L. Wu and S.-T. Lee, *Nano Lett*., **9**, 3704 (2009).
13. M.C. Putnam, S.W. Boettcher, M.D. Kelzenberg, D.B. Turner-Evans, J.M. Spurgeon, E.L. Warren, R.M. Briggs, N.S. Lewis and H.A. Atwater, *Energ. Environ. Sci*., **3**, 1037 (2010).
14. S.W. Boettcher, J.M. Spurgeon, M.C. Putnam, E.L. Warren, D.B. Turner-Evans, M.D. Kelzenberg, J.R. Maiolo, H.A. Atwater and N.S. Lewis, *Science*, **327**, 185 (2010).
15. K.Q. Peng and S.T. Lee, *Adv. Mater*., **23**, 198 (2011).
16. X. Wang, K.Q. Peng, X.J. Pan, X. Chen, Y. Yang, L. Li, X.-M. Meng, W.-J. Zhang and S.-T. Lee, *Angew. Chem. Int. Ed*., **50**, 9861 (2011).
17. P.C. Dai, J. Xie, M.T. Mayer, X. Yang, J. Zhan and D. Wang, *Angew. Chem. Int. Ed*., **52**, 11119 (2013).
18. S.W. Boettcher, E.L. Warren, M.C. Putnam, E.A. Santori, D. Turner-Evans, M.D. Kelzenberg, M.G. Walter, J.R. McKone, B.S. Brunschwig, H.A. Atwater and N.S. Lewis, *J. Am. Chem. Soc*., **133**, 1216 (2011).
19. I. Oh, J. Kye and S. Hwang, *Nano Lett*., **12**, 298 (2012).
20. E.L. Warren, J.R. McKone, H.A. Atwater, H.B. Gray and N.S. Lewis, *Energ. Environ. Sci*., **5**, 9653 (2012).
21. Y.D. Hou, B.L. Abrams, P.C.K. Vesborg, M.E. Björketun, K. Herbst, L. Bech, A.M. Setti, C.D. Damsgaard, T. Pedersen, O. Hansen, J. Rossmeisl, S. Dahl, J.K. Nørskov and I. Chorkendorff, *Nat. Mater*., **10**, 434 (2011).
22. Z.P. Huang, P. Zhong, C.F. Wang, X. Zhang and C. Zhang, *ACS Appl. Mater. Interfaces*, **5**, 1961 (2013).
23. X. Wang, K.Q. Peng, Y. Hu, F.-Q. Zhang, B. Hu, L. Li, M. Wang, X.-M. Meng and S.-T. Lee, *Nano Lett*., **14**, 18 (2014).
24. M.T. Mayer, C. Du and D.W. Wang, *J. Am. Chem. Soc*., **134**, 12406 (2012).
25. Y.J. Hwang, A. Boukai and P.D. Yang, *Nano Lett*., **9**, 410 (2009).
26. Z.Z. Xiong, M.J. Zheng, S.D. Liu, L. Ma and W. Shen, *Nanotechnology*, **24**, 265402 (2013).
27. K. Sun, Y. Jing, C. Li, X. Zhang, R. Aguinaldo, A. Kargar, K. Madsen, K. Banu, Y. Zhou, Y. Bando, Z. Liu and D. Wang, *Nanoscale*, **4**, 1515 (2012).
28. M.L. Zhang, K.Q. Peng, X. Fan, J.-S. Jie, R.-Q. Zhang, S.-T. Lee and N.-B. Wong, *J. Phys. Chem. C*, **112**, 4444 (2008).